Full Paper

Wiley Online Library

ELECTROANALYSIS

DOI: 10.1002/elan.202060246

Broadband Microwave Signal Dissipation in Nanostructured Copper Oxide at Air-Film Interface**

Papa K. Amoah,[a] Martin Košiček,[c, d] Jesus Perez,[a] Christopher E. Sunday,[a, e] Stéphane Moreau,[b] Uroš Cvelbar,[c] and Yaw S. Obeng[a]

Celebrating the 65th Birthday of Prof Emmanuel I. Iwuoha: Electrochemistry in Africa

Abstract: Contactless broadband microwave spectroscopy (a.k.a., broadband dielectric spectroscopy (BDS)) enables the accurate *operando* analysis of the electrical and magnetic properties without compromising the kinetic conditions of the experiment. The BDS method is sensitive to the actual electronic structure of species, and it is most relevant to redox reactions involving charge-transfer. In this paper, using BDS, we have studied and characterized the oxidation of a copper layer in a purposely built prototypical 3-D integrated circuit (3D-IC) during cycled high-temperature storage. We show that the microwave signal loss in these devices is attributable to the energy dissipation through the signal's interactions with the copper oxidation product. The results demonstrate that contactless BDS could be leveraged into an excellent metrology for applications that use metal oxide as sensing elements.

Keywords: Contactless broadband microwave spectroscopy · copper oxidation · high-temperature storage · microwave signal loss · energy dissipation · metal oxide · sensing elements · numerical modeling · interfacial roughness

1 Introduction

Metal oxide nanostructures (MO) have been intensively studied due to their applications in multiple fields, such as in optoelectronics, gas sensing, photovoltaics, field-effect transistors, UV lasers, and field emission sources, etc. [1]. However, the intrinsic properties of these materials are not well understood because the electrical techniques used in characterizing them invariably introduce parasitic artefacts that distort the measurands. Thus, non-contact metrology will enable an unbiased understanding of how these metal oxides actually work at the atomic level [2,3]. Contactless broadband dielectric spectroscopy (BDS) is a sensitive probe to the actual electronic structure of species. It enables the accurate operando evaluation of the electrical and magnetic properties of materials without compromising the kinetic conditions of the experiment. The BDS method is most relevant to redox reactions which involves charge transfer regardless of the nature of the charge carriers, i.e., electrons and holes [4]. Microwave signals distort when inserted into materials due to the interactions with the intrinsic electrical and magnetic properties of the material. In general, electromagnetic wave signal-material interactions result in changes in the signal's characteristics such as attenuation constant, phase constant, and propagation constant. As such, these material state-sensitive parameters can be used to monitor changes in the mechanical and chemical nature of the analyte.

Distributed element models are used to describe such signal-material interactions, because of the speeds and the frequencies involved. With these models, it is possible to describe the time-dependent variability in current along with the various circuit elements. We take advantage of these variations to extract information about the intrinsic properties of the materials under study. For example, as the materials change under external stimuli, the voltage and phase of the probing microwave signal change in response. These changes provide information about the material properties and the context of its application, e.g.,

[a] P. K. Amoah, J. Perez, C. E. Sunday, Y. S. Obeng
Physical Measurement Laboratory
National Institute of Standards and Technology
100 Bureau Drive, Gaithersburg, MD 20899
[b] S. Moreau
Univ. Grenoble Alpes, CEA, LETI, 38000 Grenoble, France.
[c] M. Košiček, U. Cvelbar
Jožef Stefan Institute, Ljubljana, Slovenia
[d] M. Košiček
Jožef Stefan International Postgraduate School, Ljubljana, Slovenia
[e] C. E. Sunday
Functional Material Group, Department of Chemical Engineering
Cape Peninsula University of Technology
Symphony Way, Bellville, 7535, Cape Town, South Africa.

[**] Certain commercial equipment, instruments, or materials are identified in this paper in order to specify the experimental procedure adequately. Such identification is not intended to imply recommendation or endorsement by the National Institute of Standards and Technology, nor is it intended to imply that the materials or equipment identified are necessarily the best available for the purpose. Contribution of the National Institute of Standards and Technology, not subject to copyright.

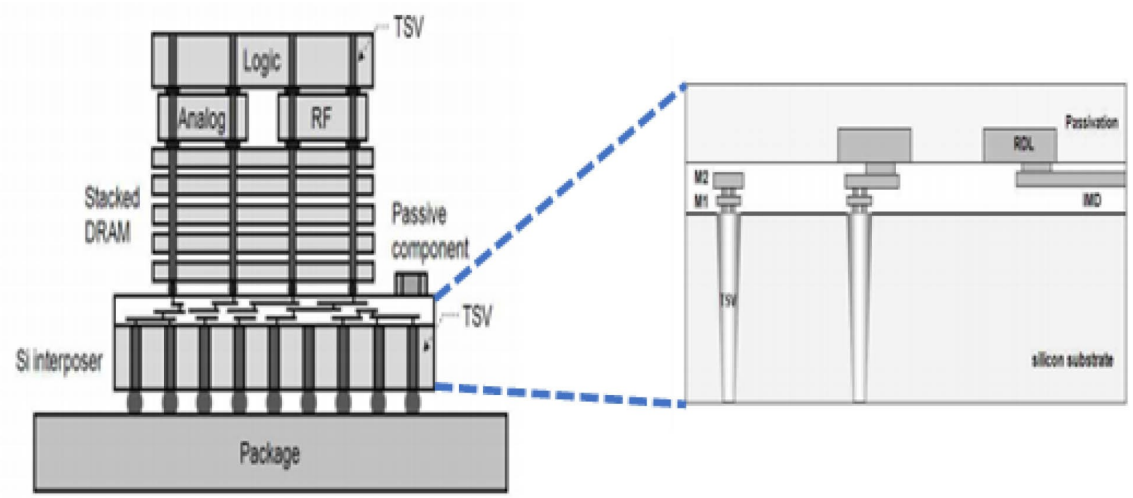

Fig. 1. A schematic cross-section of the test structure used in this work, presenting the essential components of 3D stacked IC using through-silicon via (TSV) and a silicon interposer, with a callout that shows the copper RDL layer of interest in this work (adapted from reference [7]). The called out figure is deliberately exaggerated to reveal the RDL.

construction and function in an integrated circuit packaging. In this paper, using BDS (typically in the range of 10 MHz to 40 GHz), we have studied the oxidation of a copper layer in a purposely built through-silicon via (TSV) enabled 3-D integrated circuit (3D-IC) during cycled high-temperature storage. The devices under test (DUT) were comprised of two-level stacked dies, with a Cu damascene redistribution level (RDL) that allows for circuitry fan-out and lateral communication between the chips, as shown in Figure 1 [5,6]. In this work, we specifically focused on the RDL features.

2 Experimental

The controlled oxidation of the copper layer was accomplished with modified highly accelerated temperature and humidity stress test (i.e., unbiased HAST, JEDEC Standard JESD22-A118B). The temperature was cycled between −65 °C and temperatures of 25, 75, 100 and 125 °C, respectively.

A dedicated ground-signal-ground (GSG) test structure built into the devices was used to monitor the microwave scattering data (S-parameters) in these experiments. The S-parameters were obtained with a two-port measurement configuration on a vector network analyzer (PNA–L N5230 C, 10 MHz- 40 GHz, Keysight, Inc., Santa Rosa, CA) at room temperature in an open laboratory ambient. We used the microwave signal loss between ports 1 and 2 of the vector network analyzer (i.e., RF insertion loss, S21 amplitude) to monitor the oxidation of the RDL copper interconnects. We extracted the electrical characteristics from the S-parameters of the device under test (DUT) by numerical RLCG modeling with a custom MATLAB (MathWorks, Natick, MA) code.

The direct current resistance (R_{DC}) of the oxidized RDL was obtained at room temperature by linear voltammetry (i.e., current-voltage (I–V) curves) after storing the devices overnight at room temperature in the air after thermal cycling. The overnight storing was to eliminate uncertainties in the calculated resistance due to device temperature variability.

3 Results and Discussion

3.1 Microwave Monitoring of Material Changes

Figure 2 shows the room temperature electrical resistance (R_{DC}) of the test structure as a function of peak thermal cycling temperature. The data suggest that the R_{DC} of the test structure increased with increasing thermal cycling peak temperature. This contrasts with the expected decrease in electrical resistance of copper films with thermal exposure due to secondary recrystallization of the copper [8]. The increase in R_{DC} of the Cu could be due to grain boundary "stuffing" formed by copper oxidation or segregation of impurities at the grain boundaries. The R_{DC} increase due to the grain boundary stuffing should have an upper limit due to the decreasing availability of copper grain boundaries. The secondary grain growth with thermal exposure reduces the grain boundary density. The oxidation of copper at our experimental temperatures is controlled by grain boundary diffusion [9]. Thus, the 'stuffing' phenomenon will be limited by the decreasing availability of grain boundaries, and the R_{DC} was expected to plateau with increasing thermal exposure.

Figure 3 compares the micrographs of the Copper RDL in (A) "as-received" and (B) after 4 days at 200 °C showing the development of a thick film of copper oxide film around copper trace feature. Figure 4 compares the

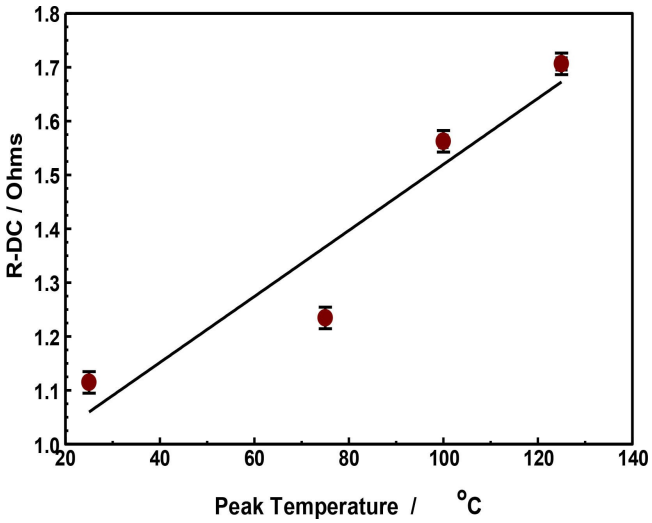

Fig. 2. Calculated room temperature direct-current resistance (R_{DC}, from direct current voltammograms) after 500 thermal cycles between −65 °C and various peak temperatures. The black line connecting the data points is a visual guide only. The error bars represent the standard deviation of the measured R_{DC} of at least four different samples.

microwave insertion loss profile of the DUTs after fixed numbers of thermal cycles, for a peak temperature of 125 °C, in the 0 to 40 GHz range. The figure shows a monotonic increase in signal loss with increasing number of thermal cycles, which suggests that the overall resistance of devices increases with increasing thermal treatment. The data is more consistent with the increased resistance of Cu RDL due to cross-section reduction from oxidation, as shown in Figure 3, than copper grain boundary stuffing. Furthermore, the formation of an oxide layer also depends on the nature of the strain at the metal-air interface. The changes in the thermo-mechanical properties of the copper interconnects with thermal cycling are of significance since local stress is known to affect the thermodynamics of copper metal oxidation [10]. We have also demonstrated elsewhere that thermal cycling results in significant increases in the mean hydrostatic stresses in the copper of TSV interconnects due to increased strain-hardening [11]. However, we note that the RDLs features studied in this work are unconstrained on three sides and can relax from the thermo-mechanical perspectives. Based on these observations, we attribute the increasing resistance to reduction of the copper film cross-section due to metal consumption during thermal oxidation of the metal.

The final oxidation product layer is composed of three regions Cu_2O, CuO, and air-filled CuO-nanofibers layer [9]. The growth of the oxidation layer is via the diffusion of either Cu ions or O ions along the boundaries of the Cu_2O grains. The driving force for copper ions diffusion from the metallic copper towards the surface-air interface can be ascribed to the net result of two synergistic chemical potential gradients, viz., (i) due to difference in oxygen partial pressure in atmospheric and in metal oxide environment, and (ii) due to stress gradient induced by the unit cell size difference between the Cu_2O and CuO [12]. The local stress and diffusion can be further increased by using plasma-assisted oxidation of copper [13]. The conductive polycrystalline copper oxide nanostructure mixtures are paramagnetic [14], and are known to absorb microwaves, mostly through dielectric loss [15]. The copper oxide layer is also redox-active. These intrinsic properties of copper oxide products could be leveraged into nanoelectronic applications [16].

As presented in Figure 5, the insertion loss (S21) increases with increasing thickness of the copper oxide film around the copper trace. Furthermore, Figure 6 displays the monotonic change in the phase angle at a discrete frequency (arbitrarily taken at 61 MHz for this work) as a function of the copper oxide thickness (i.e., number of thermal cycles at 125 °C). The changes in the phase angle are attributable to changes in the complex permittivity and permeability of the evolving copper oxide film [16]. It is obvious from the foregoing that the microwave signal loss observed in the oxidized copper

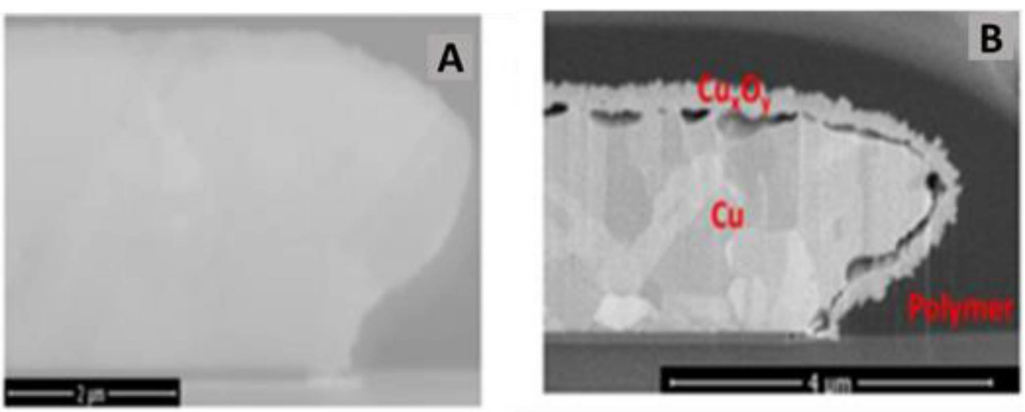

Fig. 3. Micrographs showing the development of copper oxide films around RDL feature: (A) "as-received" and (B) after 4 days at 200 °C. (Adapted from reference [17].)

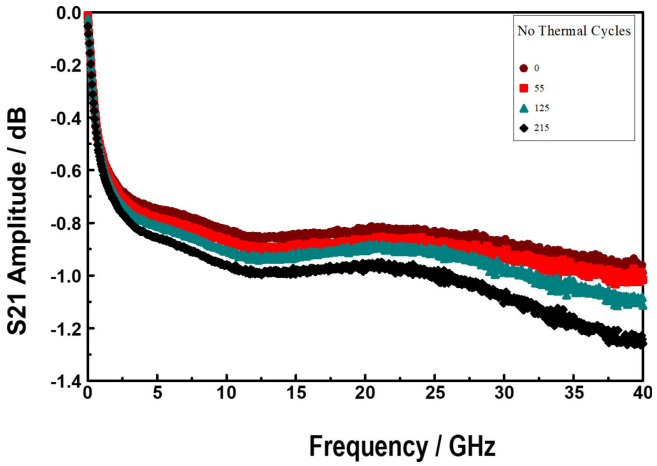

Fig. 4. Microwave Insertion loss (S21) as a function of the number of thermal cycles between −65 and 125 °C in 85 % Relative Humidity, exhibiting increasing loss with increasing cycling.

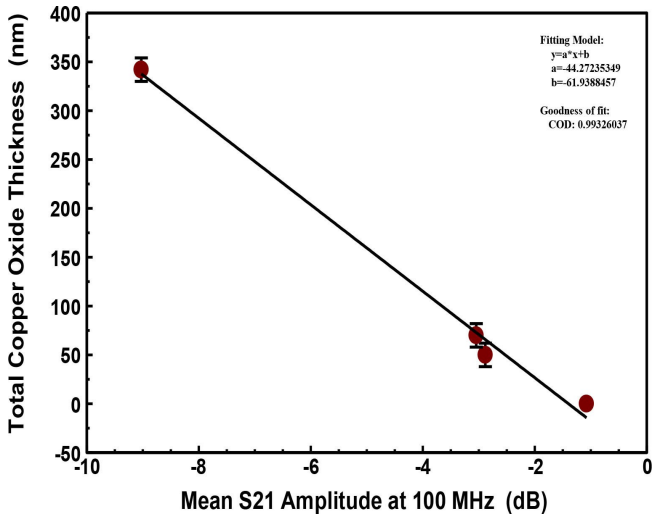

Fig. 5. Correlation between the total copper oxide film thickness and the microwave insertion loss (S21) at 100 MHz attributable to copper oxide growth around copper RDL features. The error bars represent the standard deviation of the copper oxide thickness measurements of at least six sections of SEM micrographs, such as in Figure 3.

samples in this work is due to energy dissipation in the copper oxide film formed around the Cu traces. We have previously shown that in such test structures, under extreme experimental conditions, the insertion loss may also result from significant thermo-mechanical damage [18] or accelerated materials aging [17].

Figure 7 represents a composite transverse section micrograph of an oxidized copper substrate. Raman spectroscopy reveals grading in the material composition in the copper oxide film; comprised of a Cu/ Cu_2O/CuO stack, with a filamentous quasi-one-dimensional nanostructured CuO layer at the air/film interface. In the process of thermal oxidation of copper, Copper (I) oxide

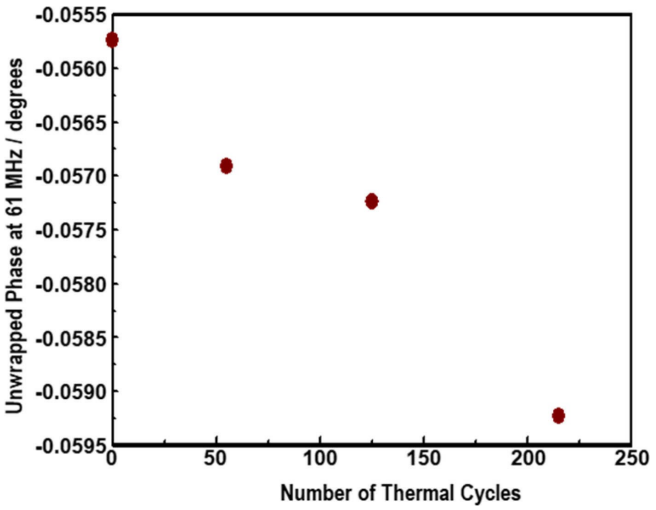

Fig. 6. Correlation between the microwave signal phase angle attributable to copper oxide growth around copper RDL features. Note: The error bars for the unwrapped phase angle are much smaller than the data symbols.

(Cu_2O) layer is first formed, followed by an intermediate compact copper (II) oxide (CuO) layer, and finally, various nanostructures potentially grow at the air-metal-oxide interface. We have demonstrated through finite element electrodynamic modeling (COMSOL Multiphysics Burlington, MA, USA) that the analytical partitioning of the microwave signal loss in such stressed DUTs required explicit accounting for the roughness of the copper oxide film formed around the copper members of the DUT, as shown in Figure 4B [19].

Figure 8 shows simulated signal attenuation as a function of the oxidized copper surface/air interface roughness (expressed as the root-mean-square (RMS) roughness); the signal attenuation increases with increasing surface roughness. At high frequencies, the microwave signal propagates mostly along the outer skin of the RDL copper. As the copper oxidizes the microwave energy is dissipated through at least three mechanisms: ohmic loss including skin effect, dielectric loss due to dipoles in the copper oxide film absorption of the microwave energy to generate heat, and radiative losses with the RDL features acting as antennae. In the skin effect, the microwave signal is absorbed at conductor surface bumps (assuming that the bumps are much smaller than the wavelength of the propagative wave [20]). The skin effect losses increase as the projected area of the coper-copper oxide interface increases due to increasing roughness. In addition, the dielectrics surrounding the RDL feature (i.e., copper oxide products) also alter the current density in the interconnects through energy storage. The relative dielectric constant, (ε_r) of copper oxidation product depends on its effective composition, thus, on the thermal history of the DUT. Based on the sensitivity analysis of the simulation results presented in Figure 8, we postulate that the dielectric loss dominates above 2 GHz. We note that

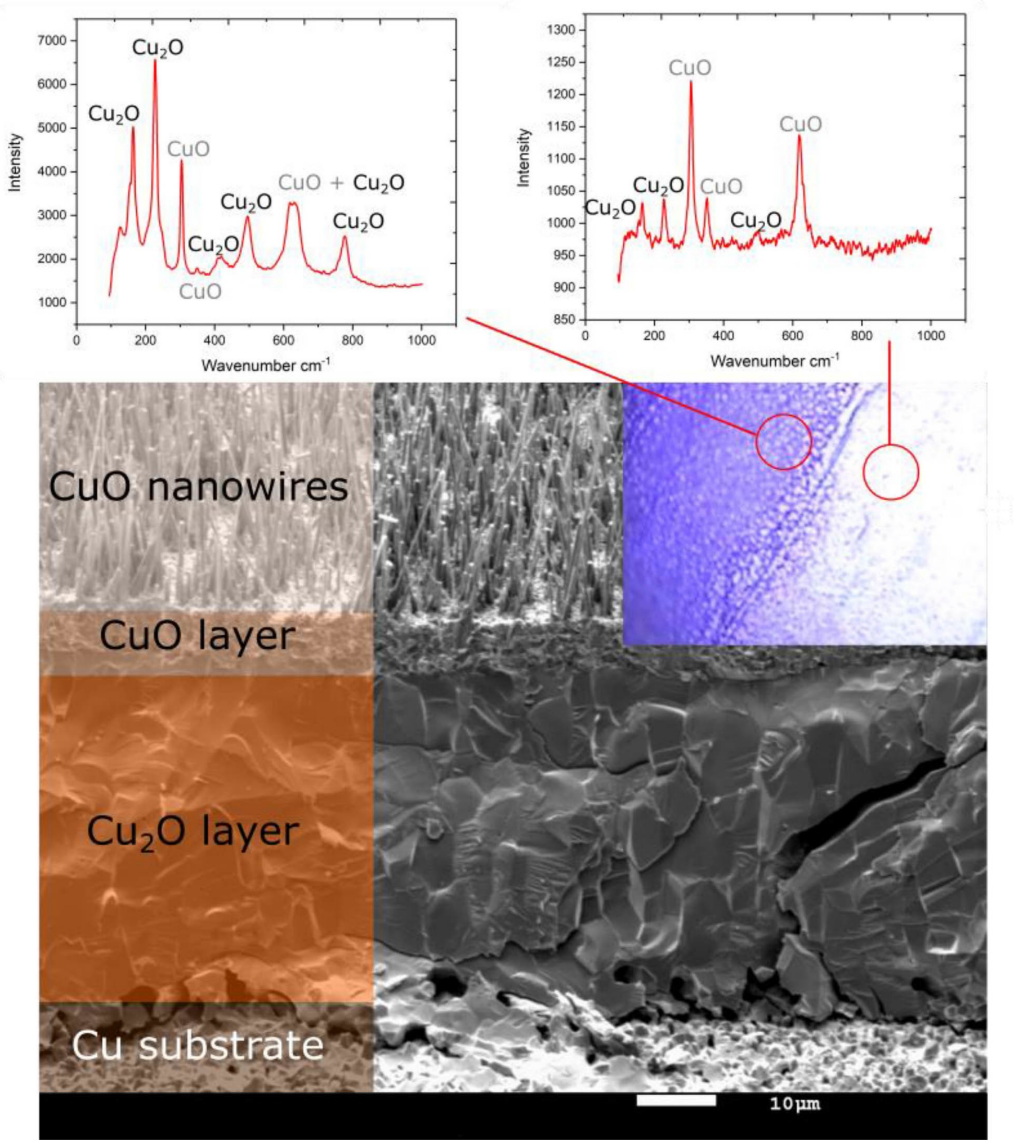

Fig. 7. A composite transverse micrograph and Raman spectra showing two types of oxides form on the surface of the copper during oxidation: CuO and Cu_2O.

our simulation results may not be accurate, since the finite element solvers we used were not optimized for broad-band microwave applications. However, the skin effect simulations are reasonably accurate

4 Perspective: Microwave Monitoring of Metal Oxide in Sensing Applications

Having characterized microwave signal propagation in copper-oxide films, we now discuss some potential electroanalytical applications of microwave spectroscopy in metal-oxides. Specifically, in this section, we discuss microwave monitoring of reactions of metal-oxides, with a focus on copper-oxide, in gas and bioanalytical sensing applications. The premise of this section is the microwave energy dissipation in metal-oxide films change due to changes in their dielectric, magnetic, electromagnetic impedance, and the microstructure in response to charge transfer reactions with other redox-active species in the environment [21].

4.1 Metal Oxides in Gas Sensing

Metal-oxides (e.g., ZnO, CuO, NiO, CuO, Cr_2O_3, Co_3O_4, and Mn_3O_4) are highly sensitive to gaseous compounds such as volatile organic compounds (VOCs) and inorganic materials such as H_2S, water, etc. Their sensory responses and abilities depend on active material characteristics such as semiconductor type and morphology. Under ambient conditions, in p-type semiconductors, such as CuO, adsorbed oxygen molecules extract electrons to

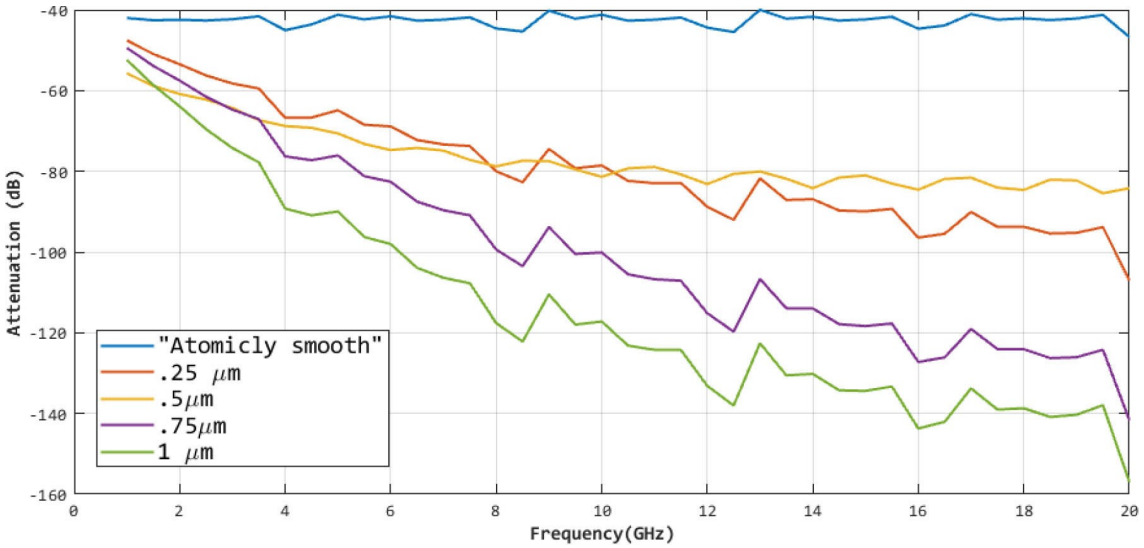

Fig. 8. Graphical summary of COMSOL simulations comparing the impact of Roughness of Cu_2O/CuO/ Air Interface on Microwave Signal Attenuation.

cause further hole formation on the surface of active sensing material, resulting in increased electrical resistance (R_{DC}) of the sensing element [22]. When oxidizing gasses, such as NO_2 or O_2, are introduced, they will withdraw even more electrons from active sites in the sensor and further decrease its resistivity. On the other hand, when reducing gasses, such as H_2S, are introduced, they donate electrons into the holes on the surface of the sensing material and thus increase its resistivity. These electron transfer processes set up dipoles on the surface of the MO [23], which induce microwave signal loss through dielectric heating [24]. The signal loss is characteristic of the electronic structure of the interfaces involved. For sensors based on CuO, the nanofilaments (1-D nanomaterials) at the film /air interface represent the optimal morphology, as they exhibit large surface to volume ratio. Indeed, nanowires (NWs) (as shown in Figure 7) have demonstrated very low detection limit for H_2S; 10 ppb H_2S detection has been achieved [25].

The sensing abilities of metal oxides can be tuned by mixing them with other oxides, as was demonstrated by [22,26]. These electron transfer processes create dipoles that are responsive to microwave probing. The sensing capabilities of these p-type semiconductors can be further improved either by controlling the carrier concentration through aliovalent doping, doping/loading the sensor material with oxide or noble metal catalysts or forming a junction between p- and n-type oxide semiconductors [27]. For example, the sensing abilities of CuO for oxidizing gasses can be further improved by decorating the CuO nanowires with TiO_2 nanoparticles (NPs), while the sensing capability for reducing gases is reduced [22]. Addition of n-type TiO_2 nanoparticles results in the formation of p-n junctions on TiO_2–CuO contact, which creates a flux of electrons from TiO_2 to CuO, and flux of holes in the opposite direction. Due to the reduction of the hole accumulation layer in CuO, resistivity of the sensing material increases. Presence of electron-withdrawing oxidizing gasses increases the hole accumulation layer back to the level of CuO NWs without the TiO_2 NPs and thus drastically decrease the resistivity. On the other hand, reducing gasses further decrease the hole accumulation layer, which was already drastically suppressed by TiO_2 NPs and thus increase in resistivity is not so pronounced, therefore, sensing activity was lowered when compared to CuO NWs without TiO_2 NPs. When it comes to H_2S sensing with p-type CuO, two mechanisms were described in the literature. The first one is described above, where H_2S is reduced by oxygen species adsorbed on CuO and electrons are released in CuO to fill holes, and thus increasing CuO resistivity. However, it was found that at higher levels of H_2S, the resistivity of sensing material decreases [28]. This is the result of sulfurization of CuO in higher H_2S levels (above 5 ppm). Higher conductivity of sensing material was ascribed to the higher contact area between adjacent nanowires induced by copper sulfide formation. However, the higher conductivity of copper sulfide may also be the reason. All these charge transfer processes alter the physico-chemical properties of the CuO, including changes in the magnetic properties, and hence its interaction with microwaves [29].

Such media supported metal oxides are advantageous in affording larger surface to volume ratios, thus presenting larger reactive surfaces for gas interaction [15,30]. A nanostructured CuO supported on semiconducting polymer membrane, such as cellulose, for gas sensing, has been demonstrated. However, these sensing applications depend on monitoring changes in electrical resistance with a circuit containing the MO-sensor, and are limited by the parasitic artefacts in the circuit such as erratic contact resistances between MO-electrode and the other electrical elements in the measurement circuit. Such

connections hamper the accurate determination of absolute resistance and relative changes that are needed for a rigorous and quantitative correlation of charge transport and catalytic properties. We suggest that non-contact BDS may be a better metrology for such a sensing application [31]. We have independently investigated and characterized cellulosic paper [32,33], which, when combined with metal oxides, could be suitable for cost-effective microwave monitored gas sensing applications. From our experience, the paper substrate for metal oxide support must be carefully chosen for BDS monitoring.

4.2 BDS Monitoring of Metal-oxide Nanostructures in Bio-applications

4.2.1 Metal-oxide Nanostructures in Disinfection

In the era of the viral pandemic, there is a heightened need for technology that improves the efficacy of personal protective equipment (PPE), such as respiratory face masks, etc. Metal oxides (MO) are known to have antiviral and other biocidal properties, copper oxide impregnated polymeric materials for PPE applications have been introduced. CuO impregnated face masks have been demonstrated to have significantly higher direct contact inactivation of both the human influenza A virus and avian influenza virus in comparison to control masks [34]. The antibacterial activity of CuO nanoparticles is generally attributed to the released Cu (II) ions, but uncertainties remain about their mechanism of toxic action. Cu-based nanoparticles may undergo profound charge-transfer transformations, under different biological and environmental conditions, which can induce significant changes in their structural and physicochemical properties and in turn, affect their toxicity. For example, depending on the amino-acidic side chain, ligands attach to the surface of CuO nanoparticles and/or alter their properties [35]. In principle, like the paper-supported MO for sensing application discussed above, non-contact BDS has the potential for monitoring the quality and capacity of such MO-impregnated PPE, as well as identify the pathogens the wearer of the PPE has been exposed to. This is possible due to the changes in the physicochemical properties of the metal oxide when exposed to biomolecules [36].

4.2.2 Metal Oxides in Electrogenerated chemiluminescence (ECL)

Electrogenerated chemiluminescence (ECL) involves the reaction of electrogenerated species to form excited luminophores, usually via an energetic redox reaction. ECL, when combined with other bioanalytical techniques, affords stupendous increases in sensitivity, by several logs of dynamic range, and provide advantages over other assays based on radio-isotopic labels, fluorescence, enzymatic activity, etc. [37]. The detection of emission in monolayer films on metallic and degenerate semiconductor surfaces showed that emission from the excited states generated by electron transfer could compete with quenching by the electrode. Potential applications of such films include active displays and means of trace analysis [38]. By adsorption of the ECL-active molecule on the surface of the electrode, significant increases in sensitivity should be possible [39]. An ECL sensor fabricated by immobilizing $Ru(bpy)_3^{2+}$-modified CuO nanoparticles (NPs) on a TiO_2 nanotube array (TN) electrode has displayed a 30% enhanced ECL signal, and a detection limit of 9.6×10^{-10} M of tripropylamine (TPA [40]). The addition of the CuO to the n-type TiO_2 nanotubes results in the formation of p-n junctions on TiO_2–CuO contact, which creates a flux of electrons from TiO_2 to CuO, and flux of holes in the opposite direction. This changes the energetics of the redox reactions with the $Ru(bpy)_3^{2+}$ moiety. The charge transfer processes are readily monitored with non-contact microwave spectroscopy. Microwaves could be used to probe the electrode solution interface to acquire further mechanistic insights and potentially enhance the efficiency of the redox processes. Such non-contact sensing will enable remote monitoring in many areas of science including, but not limited to, environmental microbiology, virology, neurobiology, molecular biology, immunology, study, and treatment of infectious diseases [37].

5 Conclusions

Using non-contact microwave spectroscopy, we have studied the oxidation in copper-based interconnects at relatively low temperatures, around 150 °C, and showed that the roughness at the air interface is due to a composite film comprised of $Cu/Cu_2O/CuO/CuO$-nanofibers. The copper-oxide oxidation product is very redox-active and effectively dissipates microwave energy. The charge transfer reactions change the electrical properties of the copper oxide films and their microwave propagation characteristics; the extent of microwave signal loss; and loss characteristics depend on the exact physicochemical properties of the copper oxide film. We propose to leverage the changes in the microwave signal to extract analytical information about a variety of systems, such as study of material aging, gas sensing and, biomedical sensing.

Data Availability Statement

The datasets generated during and/or analysed during the current study are available from the corresponding author on reasonable request.

References

[1] *Metal Oxide Nanostructures and their Applications*, ed. Y.-B. H. Ahmad Umar. American Scientific Publishers, CA, USA, (http://www.aspbs.com/mona/).

[2] N. G. Orji, et al., *Nature Electronics* **2018**, *1*, 532–547.
[3] Y. S. Obeng, *ECS Journal of Solid State Science and Technology* **2015**, *5*, P3025-P3030.
[4] A. M. Wernbacher, et al., *J. Phys. Chem. C* **2019**, *123*, 8005–8017.
[5] R. Mahajan, B. Sankman, *3D Packaging Architectures and Assembly Process Design.* In: Li Y., Goyal D. (eds) 3D Microelectronic Packaging. Springer Series in Advanced Microelectronics, vol 57. Springer, Cham. https://doi.org/10.1007/978-3-319-44586-1_2.
[6] T. Frank, et al., *Microelectronics Reliability* **2013**, *53*, 17–29.
[7] K. Yoon et al., "Modeling and analysis of coupling between TSVs, metal, and RDL interconnects in TSV-based 3D IC with silicon interposer," 2009 11th Electronics Packaging Technology Conference, Singapore, 2009, pp. 702–706, doi: 10.1109/EPTC.2009.5416458..
[8] S. Kang, et al., *J. Electron. Mater.* **2001**, *30*, 1506–1512.
[9] S.-K. Lee, H.-C. Hsu, W.-H. Tuan, *Materials Research* **2016**, *19*, 51–56.
[10] D. Kramer, Y. Wang, J. Wharton, *Faraday Discuss.* **2015**, *180*, 137–149.
[11] C. Okoro, et al., *J. Appl. Phys.* **2014**, *115*, 243509.
[12] L. Yuan, et al., *Acta Mater.* **2011**, *59*, 2491–2500.
[13] O. Baranov, G. Filipič, U. Cvelbar, *Plasma Sources Sci. Technol.* **2019**, *28.* 084002.
[14] A. A. Samokhvalov, et al., *Phys. Solid State* **1998**, *40*, 268–271.
[15] B. Guo, et al., *Nanomaterials* **2019**, *9*, 1405.
[16] M. Green, X. Chen, *Journal of Materiomics* **2019**, *5*, 503–541.
[17] P. K. Amoah, et al., *ECS Journal of Solid State Science and Technology*, **2018**, *7*, N143-N149.
[18] C. Okoro, et al., *Electron Devices IEEE Transactions on*, **2013**, *60*, 2015–2021.
[19] Papa K. Amoah, Jesus Perez, Yaw S. Oben, *Application of Broadband RF Metrology to Integrated Circuit Interconnect Reliability Analyses: Monitoring Copper Interconnect Corrosion in 3D-ICs,. in Proceedings of the 2020 International Conference on Microelectronic Test Structures, April 6–9,, Session 7.5.* **2020**, Edinburgh, United Kingdom: IEEE.
[20] Y. Shlepnev, *Unified approach to interconnect conductor surface roughness modelling. in 2017 IEEE 26th Conference on Electrical Performance of Electronic Packaging and Systems (EPEPS).* **2017**.
[21] X. F. Zhang, et al., *Appl. Phys. Lett.* **2006**, *89*, 053115.
[22] S.-W. Choi, et al., *J. Mater. Chem. C* **2014**, *2*, 8911–8917.
[23] T. I. Barry, F. S. Stone, *Proceedings of the Royal Society of London. Series A, Mathematical and Physical Sciences* **1960**, *255*, 124–144.
[24] D. Stuerga, *Microwave-Material Interactions and Dielectric Properties, Key Ingredients for Mastery of Chemical Microwave Processes*, in *Microwaves in Organic Synthesis.* A. Loupy (Ed.). p. 1–61 doi:10.1002/9783527619559.ch1.
[25] S. Steinhauer, et al., *Sens. Actuators B* **2013**, *186*, 550–556.
[26] Y. Wang, et al., *Sens. Actuators B* **2015**, *209*, 515–523.
[27] H.-J. Kim, J.-H. Lee, *Sens. Actuators B* **2014**, *192*, 607–627.
[28] J. Chen, et al., *J. Phys. Chem. C* **2008**, *112*, 16017–16021.
[29] A. Rydosz, A. Brudnik, K. Staszek, *Materials* **2019**, *12*, 13.
[30] W. Hittini, et al., *Sci. Rep.* **2020**, *10*, 2940.
[31] C. Heine, et al., *Applied Physics A* **2013**, *112*: 289–296.
[32] M. Kombolias, et al., *Anal. Lett.* **2020**, *53*, 424–435.
[33] M. Kombolias, et al., *Tappi journal* **2018**, *17*, 501–506.
[34] G. Borkow, et al., *PLoS One* **2010**, *5*, e11295.
[35] E. Badetti, et al., *Nanomaterials* **2019**, *9, 792*.
[36] M. J. Limo, et al., *Chem. Rev.* **2018**, *118*, 11118–11193.
[37] P. W. Rhyne, et al., *Bioanalysis* **2009**, *1*, 919–935.
[38] W. Miao, *Chem. Rev.* **2008**, *108*, 2506–2553.
[39] Y. S. Obeng, A. J. Bard, *Langmuir* **1991**, *7*, 195–201.
[40] Z. Yan, et al., *Electroanalysis* **2014**, *26*, 2017–2022.

Received: August 28, 2020
Accepted: August 31, 2020
Published online on ■■, ■■

FULL PAPER